Chem. Senses 29: 763–773, 2004 doi:10.1093/chemse/bjh079

Experimental and Numerical Determination of Odorant Solubility in Nasal and Olfactory Mucosa

Daniel B. Kurtz[1], Kai Zhao[2], David E. Hornung[3,4] and Peter Scherer[2]

[1]Biology Department, Utica College, 1600 Burrstone Road, Utica, NY 13502, USA, [2]Bioengineering Department, University of Pennsylvania, RM 120 Hayden Hall, 3320 Smith Walk, Philadelphia, PA 19104, USA, [3]Department of Biology, St Lawrence University, Canton, NY 13617, USA and [4]Department of Neuroscience and Physiology, SUNY Upstate Medical University, Syracuse, NY 13210, USA

Correspondence to be sent to: Daniel Kurtz, Biology Department, Utica College, 1600 Burrstone Road, Utica, NY 13502, USA. e-mail: dkurtz@twcny.rr.com and dkurtz@utica.edu

Abstract

Odorant deposition in the nasal and olfactory mucosas is dependent on a number of factors including local air/odorant flow distribution patterns, odorant mucosal solubility and odorant diffusive transport in the mucosa. Although many of these factors are difficult to measure, mucosal solubility in the bullfrog mucus has been experimentally determined for a few odorants. In the present study an experimental procedure was combined with computational fluid dynamic (CFD) techniques to further describe some of the factors that govern odorant mucosal deposition. The fraction of odorant absorbed by the nasal mucosa (η) was experimentally determined for a number of odorants by measuring the concentration drop between odorant 'blown' into one nostril and that exiting the contralateral nostril while the subject performed a velopharyngeal closure. Odorant concentrations were measured with a photoionization detector. Odorants were delivered to the nostrils at flow rates of 3.33 and 10 l/min. The velopharyngeal closure nasal air/odorant flows were then simulated using CFD techniques in a 3-D anatomically accurate human nose modeland the mucosal odorant uptake was numerically calculated. The comparison between the numerical simulations and the experimental results lead to an estimation of the human mucosal odorant solubility and the mucosal effective diffusive transport resistance. The results of the study suggest that the increase in diffusive resistance of the mucosal layer over that of a thin layer of water seemed to be general and non-odorant-specific; however, the mucosa solubility was odorant specific and usually followed the trend that odorants with lower water solubility were more soluble in the mucosa than would be predicted from water solubility alone. The ability of this approach to model odorant movement in the nasal cavity was evaluated by comparison of the model output with known values of odorant mucosa solubility.

Key words: nasal mucosa, odorant solubility, olfactory mucosa

Introduction

The initial events in olfaction consist of the movement of odorant molecules from the environment to the olfactory receptors. In the vertebrate nose, these events include the transport of the molecules of a volatile compound to the airspace above the olfactory receptors and then the transfer of at least a portion of these molecules into the olfactory mucosa. Once in the olfactory mucosa, these odorant molecules are in position to stimulate the olfactory receptors. Understanding these events requires knowledge of both the airflow dynamics and the mass transport of the gaseous odorant from the air stream to the mucus overlaying the receptive surface. Among other variables, the transport is governed by the solubility of the odorant within the nasal mucosa. As a first approximation, odorant mucosa solubility can be predicted from published values of water solubility. For example, Mozell and Hornung (1985) have shown that odorant mucus and mucosa solubility is well approximated by water solubility for odorants that are highly water soluble. However, for odorants with low water solubility, mucus and mucosa solubility can be increased by orders of magnitude over measured water solubility. The difference could result from odorant molecules dissolved in the mucopolysaccharides and lipophilic carrier proteins contained in the secretions of Bowman's glands and the sustentacular cells.

Radioisotopes have been used to measure odorant deposi-

tion in the olfactory mucosa in bullfrogs. From these depositions odorant mucosa solubility can be calculated (Hornung *et al.*, 1980, 1987); however, this work has been performed for only a very few odorants and these techniques are too invasive to be performed in humans.

Even with known odorant mucosa solubility, some of the processes involved in the transport of the odorant molecules to the olfactory receptors are resistant to direct measurement. For instance, measurement of the volume flow rate at the external naris is easily determined whereas airflow within the nasal cavity and odorant mucosal diffusivity are much more difficult to measure. The marriage of classical physiology and the modern techniques of finite element computational fluid dynamics (CFD) holds the promise of allowing for a much better description of these peripheral processes than has heretofore been possible. For example, because the information was unavailable by any other means, CFD was recently used to model odorant mass transport and airflow processes in the human nasal cavity using anatomically accurate finite element 3-D nasal cavity models (Keyhani *et al.*, 1995, 1997; Subramaniam *et al.*, 1999; Zhao *et al.*, 2004).

Combined with the numerical modeling technique, the current study took a less direct experimental route to the determination of odorant mucosal solubility and odorant transport in the human nose. As odorant was sorbed onto the mucosal surface, the mucosal concentration increased and the air phase concentration decreased along the flow path. Total odorant mucosal deposition rate was then calculated from the air phase concentration of an odorant as it entered one nostril and exited the contralateral one during a velopharyngeal maneuver. The CFD technique was applied to simulate the airflow and local odorant deposition in an anatomically accurate nasal cavity model and to predict odorant solubility and diffusive transport rate in the human nasal mucosa. The accuracy of this calculation was then tested through the comparison of the model output with known values of odorant mucosal solubility.

Materials and methods

Overview

The Experimental section of this paper describes a procedure in which the fraction of odorant removed was directly measured. Because the later Numerical Analysis (modeling) section requires a consideration of the fraction removed data, the methods and results with some preliminary discussion for the Experimental sections are discussed first. The Numerical Analysis section then follows with its own methods and results.

Experimental

Subjects

Ten females and four males served as subjects. Although most were in their twenties, subjects ranged from 20 to 56 years of age (average age = 30.2, SD = 11.3). No subject reported any symptoms of upper respiratory infection and each subject could breathe freely through her/his nose. The nasal mucosa of each subject was moist, flat and pink as evaluated during an anterior nasal exam conducted just prior to testing. All subjects signed an informed consent document that was approved by the SUNY Upstate Medical University IRBPHS.

Table 1 List of odorants

Odorant (common odorant name)	Dilution (%)
Amyl acetate (banana)	30
Benzaldehyde (almond)	10
Butanol	10
r-Carvone (mint)	10
Diphenyl oxide	25
Heptaldehyde	5
Isopropyl (rubbing) alcohol	5
D-limonene (orange)	5
Naphthalene (mothballs)	4
Nonane	10

Stimuli

The odorants listed in Table 1 were delivered to the subjects via an air-dilution olfactometer (Walker *et al.*, 1990). The concentrations are expressed as percentage dilutions of saturated vapors. Odorant saturators were constructed of 3 in. diameter Delrin pipe, capped at the ends, fitted with tubing connectors and filled with ~300 g of activated carbon saturated with liquid odorant. This activated carbon created a very large surface area from which the odorant could evaporate. While vapor saturation was not verified directly, control experiments confirmed that odorant concentration varied systematically as expected by altering the ratio of odorant airflow to dilution airflow. Odorants were chosen based on the sensitivity of the detection device (photo-ionization detector or PID) and previous work measuring odorant mucosal solubility (Mozell and Jagodowicz, 1973; Hornung *et al.*, 1980, 1987).

Procedure

Odorants were introduced into the right nostril via a Teflon nasal olive connected to the output of the olfactometer (see Figure 1) (Hornung *et al.*, 1980, 1987). Subjects performed a velopharyngeal closure to prevent the odorant from entering the oral cavity. Between trials, odor-free air flowed into the right nostril and out of the left nostril. The left nostril was connected to another nasal olive that was vented to the room exhaust. A PID (HNU Systems) was connected to the exhaust tubing exiting the left nostril and continually

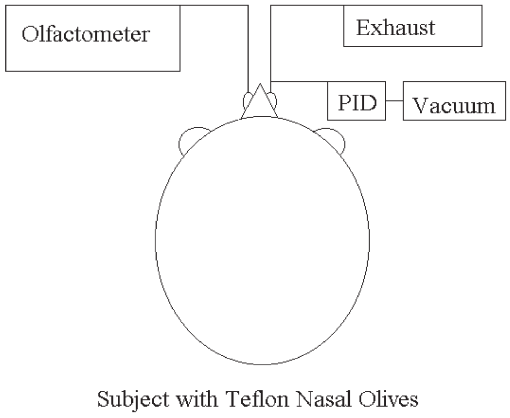

Figure 1 Diagram of the experimental procedure.

sampled air/odorant at a rate of 100 cm^3/min. Upon the initiation of a trial, odorant concentration (change in PID output voltage) was recorded at 10 and at 20 s after the start of stimulus presentation.

To control for odorant absorption by the olfactometer tubing, odorant concentration was also measured at 10 and 20 s without a nose in the system by connecting the two nasal olives with a 2 cm piece of Teflon tubing (non-nasal trial). When connected in this way, it was assumed that the odorant concentration measured was the same as that which would have entered the nasal cavity, if the cavity had been in place. Thus, these measures served as a baseline against which to calculate odorant removal by the nasal cavity. Because water from the nasal cavity partially quenched the responsivity of the PID, it was important to re-humidify the PID prior to each nasal and non-nasal trial. Therefore, each trial started with the nasal cavity in place for 60 s. On the nasal trial, the airstream was then switched from air to odor. On the control (non-nasal) trials, the nasal olives were removed by the subject and connected to each other with the short piece of Teflon tubing. Immediately thereafter, the airstream was switched from air to odor and odorant concentration recorded at 10 and at 20 s after the start of stimulus presentation.

The fraction of odorant remaining in the airstream after passing through the nasal cavity was calculated as the ratio of the measured odorant concentrations with the nasal cavity in place to those measured with the nasal cavity taken out of the flow path. That is:

$$\text{fraction of odorant remaining in the airstream} = ([\text{PID voltage}_{\text{with nasal cavity}}]/[\text{PID voltage}_{\text{without nasal cavity}}])$$

The fraction of odorant remaining in the airstream was determined in triplicate for each odorant for each subject. In addition, the fraction of odorant remaining in the airstream was determined for total airflows of 3.33 and 10.0 l/min. The fraction removed from the airstream (η^{exp}) was then 1 minus the fraction of odorant remaining in the airstream.

Table 2 Average fraction of odorant remaining in the airstream (SE)

	3.33 l/min, 10 s	3.33 l/min, 20 s	10 l/min, 10 s
Amyl acetate	0.79 (0.04)	0.76 (0.05)	0.92 (0.02)
Benzaldehyde	0.18 (0.02)	0.14 (0.02)	0.32 (0.06)
Butanol	0.10 (0.01)	0.15 (0.01)	0.33 (0.03)
Carvone	0.13 (0.02)	0.09 (0.01)	0.18 (0.03)
Diphenyl oxide	0.34 (0.04)	0.32 (0.12)	0.47 (0.04)
Heptaldehyde	0.68 (0.02)	0.67 (0.02)	0.87 (0.05)
Isopropyl alcohol	0.12 (0.02)	0.18 (0.02)	0.38 (0.03)
Limonene	0.87 (0.04)	0.90 (0.04)	1.01 (0.07)
Methyl benzoate	0.10 (0.01)	0.10 (0.01)	0.32 (0.04)
Nonane	0.97 (0.05)	0.93 (0.04)	1.06 (0.08)

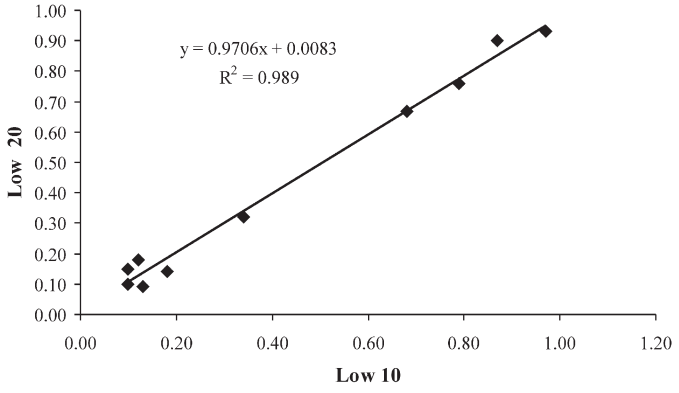

Figure 2 The fraction of odorant remaining in the airstream at 10 s plotted against that seen at 20 s (flow rate = 3.33 l/min).

Experimental results

The average fractions of odorant remaining ($1 - \eta^{exp}$) in the airstream are presented in Table 2. Standard errors are shown in parentheses. The fraction of odorant remaining varied from a low of 0.09 for carvone at 20 s at a flow rate of 3.33 l/min to a high of a little over 1 for nonane and D-limonene at the short time period and the higher flow rate.

The fraction of odorant remaining in the airstream at the lower flow rate at 20 s was nearly identical to that at 10 s. The slope of the regression line from a plot of the fraction of odorant remaining in the airstream at 10 s plotted against that remaining at 20 s (Figure 2) was very close to 1.0 and the intercept was not different from zero. This finding is important because it establishes that the outlet odorant concentration had reached a steady state within 10 s of the start of the trial and because steady state air phase odorant concentration is an important requirement of the fluid dynamic modeling seen later. (Note that if nearly identical is defined as a difference of less than or equal to the combined standard errors, the fraction of odorant remaining in the

airstream at 20 s was not quite equal to that at 10 s for butanol, carvone and isopropyl alcohol. Over time, the fraction of odorant remaining in the airstream would be expected in rise from 0 to some steady state. For carvone, the fraction of odorant remaining in the airstream dropped and therefore likely represents experimental error. For butanol and isopropyl alcohol, the fraction of odorant remaining in the airstream increased by ~50%. These differences may represent experimental error or may reflect a longer time-course necessary to reach a steady state for these two odorants. Because of this, calculations of odorant solubility based on these three fractions must be considered estimates. However, it should be pointed out that when the differences in fraction of odorant remaining in the airstream is examined against the full range of possible fractions, the differences for butanol, carvone and isopropyl alcohol are not out of line with the other odorants. While the exact fractions of odorant remaining in the airstream for butanol, carvone and isopropyl alcohol remain to be determined precisely, their magnitudes both at 10 and 20 s relative to the other odorants seems pretty well set.)

When the flow rate of the airstream was increased from 3.33 to 10.0 l/min, the fraction of odorant remaining in the airstream increased. Figure 3 shows the relationship between the fraction of odorant remaining in the airstream for each odorant when measured at 3.33 l/min and 10.0 l/min. The slope was not different from 1.0 (95% confidence interval includes 1.0) while the *y*-intercept was significantly different from zero ($P < 0.001$, regression analysis). These findings indicate that the increase in airflow results in an increase in the fraction of odorant remaining in the airstream of ~19%, but leaves intact the relationship among odorants. This result was expected since as the flow through the nasal cavity increases, the time available for odorant to flow onto the surface of the nasal mucosa becomes shorter and less odorant is deposited on the mucosa. Thus, as flow rate increases, more odorant remained in the airstream. This finding is in agreement with previous numerical modeling results (Keyhani *et al.*, 1997).

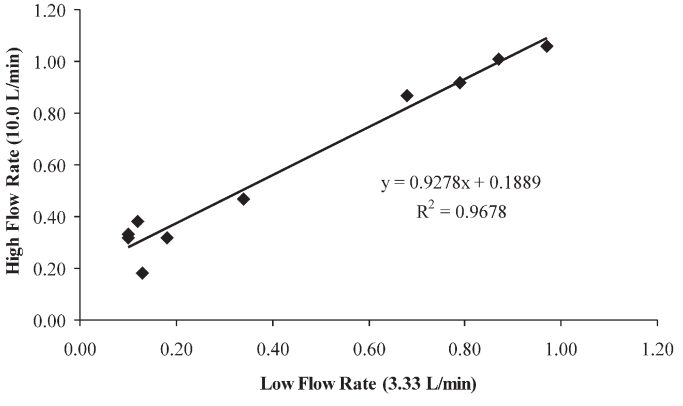

Figure 3 The fraction of odorant remaining in the airstream at the lower flow rate plotted against that seen at the higher flow rate.

The data from the higher flow rate at 20 s differed greatly from the orderly relationships seen both time periods at the low flow rate and for the short time period at the high flow rate. It is hypothesized that this is the result of evaporative drying of the PID between the 10 and 20 s data points and a removal of concomitant quenching of the PID response. A removal of quenching at 3.33 l/min was not observed until after the 20 s recording period. When the flow rate was increased to 10 l/min, the higher flow caused drying to occur faster, often before the 20 s time period but never before the 10 s time period. The data at the 20 s time period at the high flow rate were considered uninterpretable and are not presented.

Discussion of Experimental section

Although, as will be discussed in detail later, the fraction of odorant remaining in the air stream is a function of many variables, it is clearly related to the odorant's solubility in the nasal mucosa. The influence of odorant solubility on peri-receptor events has been described in a series of experiments performed in the laboratories of Mozell and Hornung (Mozell and Jagodowicz, 1973; Hornung *et al.*, 1987; Mozell *et al.*, 1987; Kent *et al.*, 1996). Central to this work is the hypothesis that the nasal cavity in the frog functions like a chromatography column. Odorants that were highly mucus soluble sorb to the mucosal surface near the external naris with little remaining in the airstream to sorb to the mucosal surface further along the flow path (Hornung and Mozell, 1977). On the other hand, odorants that are less mucosa soluble are more evenly distributed along the flow path. This differential distribution of odorant on the olfactory mucosa results in differential odorant-induced activity patterns as measured with spatially distant electrodes placed on the olfactory nerve (Mozell, 1970) or with voltage sensitive dyes placed on the olfactory mucosa (Kent *et al.*, 1996). One measure of this differential distribution was the ratio of the summated neural activity in the lateral branch (further along the flow path) to that of the medial branch (early in the flow path) of the olfactory nerve of the bullfrog. Small ratios were generated by highly mucosal soluble odorants for which most of the odorant was sorbed in the area of the medial branch while little odorant remained in the airstream to be sorbed in the area of the lateral branch. LB/MB ratios near 1.0 were generated for odorants that had low mucosa solubilities. In these odorants, mucosal deposition was minimal and, therefore, the airphase concentration remained high and constant throughout the flow path. As a result, the same stimulus was delivered to the receptors all along the flow path, producing a reasonably constant level of neural activity and an LB/MB ratio near one. [Note that although the spatial distribution of receptor cells and specific receptor proteins modifies this ratio somewhat, this effect is secondary to the effect of spatially disparate odorant deposition (Mozell, 1970).] Since both the fraction of odorant remaining in the airstream and the LB/MB ratio primarily

seem to reflect odorant mucosa solubility, we hypothesized that the fraction of odorant remaining in the airstream would be a monotonic function of the LB/MB ratio. This was proposed in spite of the fact that the two measures described the results of two very different experiments in very different vertebrates.

In Table 3, LB/MB ratios are presented from Mozell (1970) for the nine odors in common between the current study and Mozell's previous work. Also presented in Table 3 are the fractions of odorant remaining in the 3.33 l/min airstream when measured at the 20 s time point. The odorants have been sorted by the LB/MB ratio and inspection of these data show a clear relationship, namely as the LB/MB ratio increase, the fraction of odorant remaining in the airstream also increases. This relationship is shown graphically in Figure 4. While some scatter is apparent at small LB/MB ratios, a linear function accounts for nearly 97% of the total variance. It seems that the sorption of odorant molecules onto the human nasal mucosa is governed by the same principles that govern the distribution of odorant along the flow path in the olfactory sac and the resulting electrical activity in the branches of the frog olfactory nerve.

Table 3 LB/MB ratio is an inverse function of average fraction of odorant remaining in the airstream

Odorant	LB/MB ratio	Fraction of odorant remaining in the airstream
Butanol	0.01	0.15
Carvone	0.03	0.09
Methyl benzoate	0.08	0.10
Benzaldehyde	0.10	0.14
Diphenyl oxide	0.15	0.32
Heptaldehyde	0.60	0.67
Amyl acetate	0.71	0.76
Limonene	1.03	0.90
Nonane	1.03	0.93

Data are taken from Table 2; low flow rate of 3.333 l/min measured at 20 s.

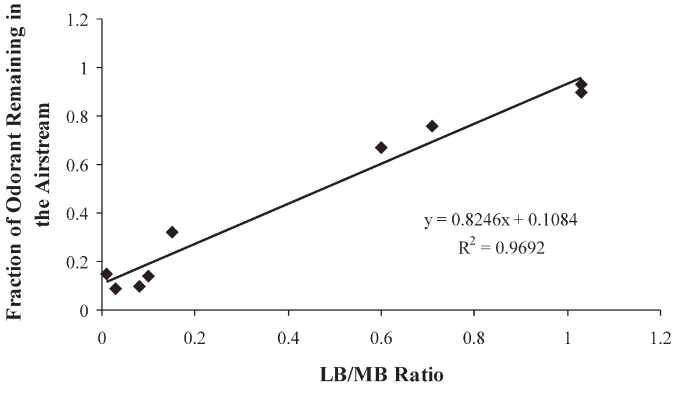

Figure 4 LB/MB ratio plotted against the fraction of odorant remaining in the airstream.

It should be noted that because the fraction of odorant remaining (or its inverse—the fraction of odorant that is removed from the airstream and sorbed into the nasal mucosa) is for mucosal uptake in both nasal cavities combined, the present measuring techniques did not allow for the measurement of mucosal uptake at specific locations in the nasal cavity (e.g. anterior olfactory region versus posterior olfactory region). Such a measure would most likely have provided an even better match with the LB/MB data. However, the high correlation between the fraction remaining under different flow rates with the LB/MB data (not shown) suggests that both measurements are reflecting the same physiochemical phenomenon and so the data would seem to be appropriate for numerical modeling.

Numerical

Constructing the 3-D numerical nasal nodel

A 3-D anatomically accurate finite element nasal model (Zhao *et al.*, 2004) that includes both sides of the human nasal cavity and the nasopharynx was used to simulate nasal airflow and nasal odorant transport as previously described. The model was constructed from an axial CT (computerized tomography) of a healthy adult female (1 mm slices, 512 × 512 pixels, pixel size = 1.0 × 0.3906 × 0.3906 mm). This model can be thought of as a shell of the nasal cavity in which the outer surface of this shell is the air/mucosa interface and the inside of the shell is empty. Airflow and odorant concentration in this empty space was modeled in part by filling this space with ~1.7 million tetrahedral elements.

Briefly, for the first stage in the modeling, the interface between the nasal mucosa and the air in the nasal cavity was delineated with software designed to manipulate computerized images (AMIRA®; Mercury Computer Systems, Los Angeles, CA). A mesh filling the nasal cavity air space was then created from tetrahedral elements with a grid generation program (ICEM®; ICEM CFD Engineering, Berkley, CA). A finer mesh was created near the mucosal surface to more accurately model the rapidly changing air velocity and odorant concentration in that region (Zhao *et al.*, 2004).

Next, laminar airflow (Keyhani *et al.*, 1995; Zhao *et al.*, 2004) was modeled with a program to perform finite volume numerical analysis (Fluent©; Fluent Inc., USA). To model the experimental procedure described above, air was mathematically drawn into the right nostril by an imposed air pressure and allowed to flow out the left nostril with the naso-pharynx closed at the experimental flow rates of 3.3 and 10.0 l/min. Figure 5 shows the resulting modeled airflow steam lines as viewed from the floor of the nasal cavity looking superiorly.

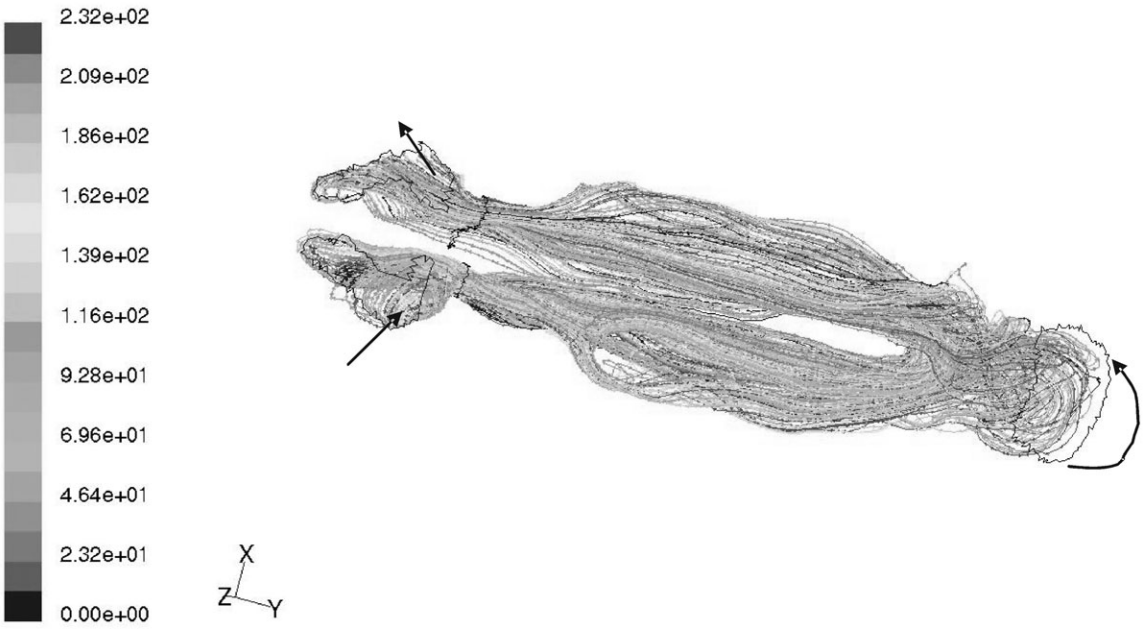

Figure 5 Streamline pattern for computed steady laminar airflow into right nostril and out of the left nostril. The nasal cavity is viewed from below looking superiorly.

Odorant mass transport

The steady state uptake of odorant onto the mucosa was determined by three dimensionless parameters, the Schmidt number $Sc = D_a/\nu$, the Reynolds number $Re = Ud_{in}/\nu$ and the homogeneous wall mass transfer parameter K (Hahn *et al.*, 1994; Keyhani *et al.*, 1997), in which D_a is the odorant diffusion coefficient in air, ν is the kinematic viscosity of air (1.7894×10^{-2} kg/m·s), U is the airflow velocity and d_{in} is the characteristic length of the nasal cavity. The Sc and Re number for each odorant flow are known but K is unknown. If values for all three parameters were known, it would be possible to simulate the fraction of odorant removed from the airstream (η^{cal}) in the nasal cavity using the airflow field described in the previous paragraph. To approximate the K for each odorant, a numerical simulation for various values of K at a given flow rate was used to generate a curve of the computed fraction of odorant removed from the airstream with velopharyngeal closure (η^{cal}) versus K (Figure 6). In this figure, η^{cal} was plotted as a function of the log(K). The K value for any given experimental odorant (K^{exp}) could be approximated by matching the experimental fraction of odorant removed (η^{exp}) listed in Table 2 (The example shown is for methyl benzoate (Sc = 2.2136, nasal airflow rate = 10 l/min), a K value of 22.962 matched the experimental fractional uptake value of 68%.

Air flow and odorant concentration within the nasal cavity have been modeled theoretically (Hahn *et al.*, 1994; Keyhani *et al.*, 1997) to predict the sorption, diffusion and removal of odorants in the mucosal lining. The basic

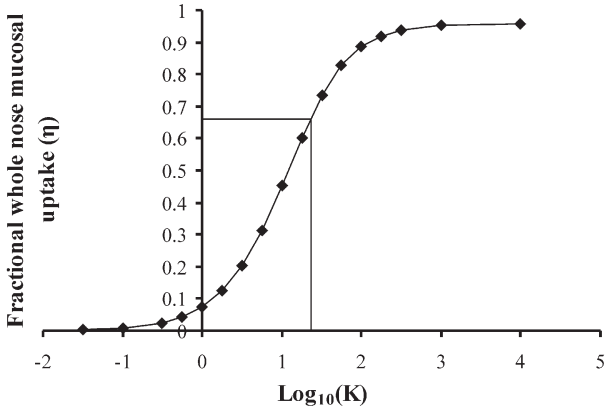

Figure 6 Approximation of K for each odorant (shown is methyl benzoate) from the fraction of odorant removed from the nasal cavity.

premise of these models was to simplify the human mucosal environment into layers of compartments: airphase, mucus, cell layer, submucosal blood compartment, etc.

From the numerical models that were created to simulate this simplified physical model, it was possible to estimate the K value based on the physiochemical properties of the mucosa and odorant molecules. Based on the assumption of a steady state (importantly, a condition that has been established for the current experimental data; see Figure 2) odorant flux through the mucosal layer, Keyhani *et al.* (1997) showed that odorant gas concentration satisfies the mixed boundary condition at the mucosal wall:

$$\frac{\partial C'}{\partial y'} + KC' = 0, \text{ at } y = 0 \quad (1)$$

where in the simplest case K for an odorant is given as

$$K^{\text{cal}} = \frac{d_{\text{in}} D_{\text{m}}}{D_{\text{a}} \beta H_{\text{m}}} \quad (2)$$

in which the mucosal layer is represented as a single homogeneous compartment. In this equation, d_{in} is the hydraulic diameter (4 × area/perimeter) of the nostril, D_{m} is the odorant diffusion coefficient in mucosa, β is the air/mucus odorant partition coefficient (defined by the ratio of odorant concentration in airphase to the concentration in mucus near the air/mucus interface) and H_{m} is the thickness of the mucosal layer and also the length of path that odorant molecules need to diffuse through. D_{a} represents the diffusivity of odorant molecules through air. Values of D_{a} (see Table 4) could be determined by the Wilke–Chang equation [used to predict molecular diffusion in diluted mixtures (Welty *et al.*, 1976)]; accurate values of β_{exp} have been determined experimentally in frog mucosa (Hornung *et al.*, 1980, 1987; Hornung and Mozell, 1981) for some odorants, but the value of this parameter is unknown for most odorants; and rough estimations exist for D_{m} (usually just the water value D_{w}) and $H_{\text{m}} \approx 30$ μm (Getchell *et al.*, 1984). These values are shown in Table 4.

The K^{exp} value obtained from fitting the experimental fraction removed data can be used to obtain information about unknown/uncertain parameters in equation (2). Two of these values (D_{m} and β) are odorant specific (see Table 4) and the last (H_{m}) is assumed to be odorant independent. Since there are three uncertain/unknown parameters in equation (2) that need to be determined from one fitted K^{exp} value per odorant, it is mathematically impossible to analytically determine them all exactly. However, the accuracy of the less well characterized variables can be evaluated. Odorants with experimentally determined β and K served as the basis to assess the accuracy of the estimations of D_{m} and H_{m}, for which only estimates exist.

In Figure 7, the fitted K^{exp} values are plotted against K^{cal} values theoretically calculated from equation (2) for the five odorants in Table 1 using their known frog mucosal solubility β_{real} and their diffusivity values in water. For the low flow rate (3.3 l/min, 20 s recording) data, a coefficient $a_{\text{K}} = 2.12 \times 20^{-2}$ was found using linear regression (with high confidence, $R^2 > 0.9$) between the experimentally found K^{exp} values and the calculated K^{cal} as

$$K^{\text{exp}} = a_{\text{K}} K^{\text{cal}} = (1/47) K^{\text{cal}} \quad (3)$$

In equation (3), if it is assumed that humans and bullfrogs have the same mucosal solubility β_{real}, the difference between K^{exp} and K^{cal} in equation (3) is due only to the

Table 4 Physical properties for a number of odorants (at 25°C and 1 atm)

Odorant	D_{a} (cm^2 s^{-1})[b]	$D_{\text{m}} \times 10^5$ (cm^2 s^{-1})[c]	β (air/water)[d]	β (air/mucus)
Carvone[a]	0.062	0.69	3.13E–03	1.30E–04[f]
D-limonene[a]	0.063	0.70	1.04E+00	6.00E–03[f]
Benzaldehyde[a]	0.079	0.91	1.08E–03	5.00E–04[f]
Amyl acetate[a]	0.067	0.78	1.57E–02	2.50E–03[e]
n-Octane	0.060	0.74	1.30E+02	4.80E–01[g]
Geraniol	0.058	0.67	2.42E–03	1.00E–03[f]
1-Butanol[a]	0.091	0.98	3.57E–04	3.40E–04[e]
Isobutyric acid			5.10E–05	5.59E–05[e]
Methyl benzoate	0.071	0.75	1.31E–03	1.74E–04[h]
Heptaldehyde	0.070	0.70	1.09E–02	1.25E–03[i]
Rubbing alcohol	0.099	0.87	3.28E–04	2.97E–04[h]
Diphenyl oxide	0.067	0.70	1.13E–02	4.15E–04[h]

D_{a}, air phase diffusivity; D_{m}, mucus diffusivity.
[a]β Values for air/mucus were used in the model to fit unknown parameters.
[b]Calculated using the Wilke–Chang equation (Welty *et al.*, 1976)
[c]Values in water. Calculated using the Fuller equation (Welty *et al.*, 1976).
[d]Howard *et al.* (1997); convert from Henry's law constant for water.
[e]Hornung *et al.* (1987); air/bullfrog nasal mucosa partition coefficients.
[f]Hornung *et al.* (1980); air/bullfrog nasal mucosa partition coefficients.
[g]Hornung *et al.* (1980); air/bullfrog nasal mucosa partition coefficients.
[h]Numerical calculated air/mucus partition coefficients.

difference between the values for D_m and H_m in water versus in that seen in human mucus. Equation (3) can then be rewritten as:

$$\frac{d_{in}D_m^{real}}{D_a H_m^{real}\beta_m^{real}} = K^{exp} = a_K K^{cal} = a_K \frac{d_{in}D_w}{D_a H_m^{cal}\beta_m^{real}} \quad (4)$$

Using the first and last terms in equation (4) and canceling out the symbols in common, the difference between K^{exp} and K^{cal} can be generalized by defining the permeability of the human mucosa to an odorant as:

$$\text{Permeability} = \frac{D_m^{real}}{H_m^{real}} = a_K \frac{D_w}{H_m^{cal}} \text{ or } = P^{real} = a_K P^{cal} \quad (5)$$

and the effective diffusive resistance of the mucosal layer to odorant diffusion as:

$$R = \frac{H_m^{real}}{D_m^{real}} = \frac{H_m^{cal}}{a_K D_w} \text{ or } = R^{real} = \frac{R^{cal}}{a_K} \quad (6)$$

The introduction of the term 'effective diffusive resistance' or its inverse 'permeability' is because the decrease of odorant mucosal diffusive flux could be a result of either the increase in diffusive path (H_m) and/or the decrease of odorant diffusivity in mucosal layer (D_m), since they appear together in equation (2) as H_m/D_m. Thus, H_m and D_m were combined in equations (5) and (6) to describe the ease with which odorants move through the mucosal layer.

Finally, equating the second and last terms in equation (4):

$$\beta_m^{real} = \frac{a_K d_{in} D_w}{K^{exp} D_a H_m^{cal}} \quad (7)$$

gives the air/mucosa partition coefficient of an odorant as a function of the experimentally determined fraction of odorant removed from the airstream (and the currently available estimates of D_{in}, D_w, D_a and H_m). Equation (7) was then applied to generate partition coefficients for the four odorants for which the fraction of odorant removed from the human nasal cavity was experimentally determined and for which previous estimated of the partition coefficient were based on water solubility. Calculated partition coefficients are shown in Table 4.

In Figure 8, experimentally measured and calculated [last four unfilled, equation (7)] odorant air–mucus partition coefficients (β_m^{real}) are plotted against measured air–water (β_w) partition coefficients from the literature. The data points form a band just below the identity line and deviate further from the identity line with lower solubility (high β) in water. Three simple carbon chain alcohol and acid molecules, 1-butanol, isobutyric acid (measured by Hornung *et al.*, 1980) and rubbing alcohol lie on the identity line, due to their similar high solubility in both water and lipid. The next group includes a long chain alcohol (geraniol) and an acetate (amyl acetate) both of which are less soluble in water than the simple carbon chain alcohol and acid molecules listed above). The molecules of this second group appear to be more soluble in mucus than in water. The rest of the odorants that are all hydrophobic molecules with benzyl rings can be orders of magnitude more soluble in mucus than in water from both experimental references and our numerical simulation. These data provide evidence that the calculated air/mucus partition coefficients are reasonably accurate and behave in the same way as the previously measured air/mucus values. First, odorants with high water solubility also tend to be highly soluble in the nasal mucosa and, secondly, odorants with low water solubility tend to be generally more soluble in the nasal mucosa than would be predicted solely from their water solubility. The mucopolysaccharide and other hydrophilic components in the mucosa and the possible interaction with odorant binding proteins in the mucosal layer which facilitate the transport of lipophilic odorant in hydrophilic mucus (Pelosi, 1994) could be reasons for the differences in mucosal/water odorant solubility.

The high flow rate (10 l/m, 10 s) data were processed using the same approach. The results are consistent with the low flow rate data and provide the same solubility results as the low flow data, but a_K has the value 4.69×10^{-2} instead of 2.12×10^{-2}. However, since uptake of odorants in nasal mucosa scales more with log(K) than with K, a factor of 2 is a minor difference. It is hypothesized that the relationship between K^{exp} and K^{cal} can take a general linear form, as:

$$K^{exp} = a_K (K^{cal})^n$$

or

$$\log(K^{exp}) = \log(a_K) + n\log(K^{cal})$$

where the most likely value of n is 1.0. [Note that the support for $n = 1$ is not shown but was generated from linear regressions between log(K^{exp}) and log(K^{cal}).] Systematic experimental error might explain the factor of 2 difference in a_K: since a decrease in PID readout at the inlet due to a decrease in moisture at higher air flow rate could result in a measured increase in fractional whole nose mucosa uptake, and thus a higher estimated K^{exp}. A 5% error or less could result in a doubling in K^{exp}. However, since this shift is systematically observed across whole range of K values, it won't affect the β_m^{real} estimations.

Discussion

As discussed above, the combination of experimentally determined odorant removal from the nasal cavity and the finite element modeling of nasal airflow and odorant movement from the airphase to the nasal mucosa has allowed for the determination of previously unknown mucosal solubility in a set of four odorants. These solubilities are now available for the modeling of odorant/odorant interactions in the

nasal cavity and olfactory musosa and for modeling odorant delivery to the olfactory cleft. The model also points to the investigation of the process of odorant movement through the nasal mucosa.

The definition of permeability and diffusive resistance given by equations (5) and (6) allows complex diffusion and other transport processes in the mucosal layer to be modeled as that in a simple water layer of thickness H_m by adjustment of the coefficient a_K. The mechanisms for such a 47-fold increase ($1/a_K = 47$) in resistance R or decrease in mucosal permeability P compared to the value estimated for a water layer of thickness H_m could include the following.

1. Increase in length of the effective diffusion path (H_m): the mucus layer is described as consisting of a superficial watery layer estimated to be 5 μm thick and a deeper, more viscous layer (Getchell *et al.*, 1984). A dense cilliary matrix formed by either respiratory epithelium or olfactory epithelium spans the middle, which increases the tortuosity of the diffusion path, especially for non-lipid soluble odorants. These factors increase the length of the effective diffusion path (H_m).
2. Decrease in odorant diffusivity in mucus due to higher mucus viscosity than water: assuming the mucosa to be a viscous layer of viscosity μ, the Stokes–Einstein equation: $D = kT/6\pi\mu r$ (where μ is the dynamic mucosal viscosity and r is the radius of the odorant molecule) predicts a lower diffusivity for a higher mucosal viscosity. If the mucosal viscosity can be measured, then equation (5) gives:

$$\frac{\mu_w H_m^{cal}}{\mu_m H_m^{real}} = a_K$$

3. Accumulation of odorants in the mucosal layer: this could lower the mucosal-air concentration gradient, the driving force for diffusion and act as an additional diffusive resistance. The approximation in the model that the uptake of odorant by submucosal blood flow is steady state with no accumulation may not be true for all experimental conditions (Hornung and Mozell, 1981).
4. Additional resistance due to lipid membrane permeability: in reality the mucosal layer contains a variety of cell types and layers including lipid containing cell membranes and basement membrane. Odorant diffuses through all these layers and a more exact analysis would require accounting for this heterogeneity. Because the processes that contribute to diffusive resistance have not been studied in detail, these processes were combined as a single mucosal permeability or diffusive resistance.

Equation (1) (and most of the equations that follow) assume that odorant transport within the mucosa is in a quasi steady state. However, this assumption does not preclude the development of more specific models of the complex mucus–odorant interaction. Indeed, these more specific formulations should still be interpretable in terms of odorant mucosal transport resistance as in equations (5) and (6) as a summation of the processes involved in steady state mucosal odorant transport process. That is, futher development of this model is expected to extend, but not invalidate, the current model.

The linear regression in Figure 7 suggests that: (i) the increase in odorant diffusive resistance of human mucosa over that of water seems to be quite general and non-specific to the odorant used and (ii) equation 3 and a single a_K value could be a good approximation for many odorants, independent of flow rate. One possible explanation as suggested by the Stokes–Einstein equation for D is that for a given mucosal structure, odorant/mucosa diffusivity is dependent only on odorant molecular size, thus the increase in diffusive resistance of the mucosa as compared with water is mainly due to the increase of mucus viscosity and mucosal structure, which is non odorant specific. However, the odorant solubility difference between the nasal mucus and water was much more odorant specific (see Figure 8), since solute–solvent interaction depends on various properties of the odorants including: polarity, polarizability, electron-pair and hydrogen bond donor/acceptor ability, acidity/basicity, and hydrophobicity/hydrophilicity (Orozco and Luque, 2000).

To summarize, the difference between odorant transport in human nasal mucosa and in a thin layer of water seems to have two aspects: a non-odorant-dependent increase in diffusive resistance of the mucosa and an odorant-specific change in air/mucus solubility. Because of the latter, a 'universal curve' of odorant mucosal solubility versus water solubility doesn't exist for all odorants.

One important future use of the numerical model is to estimate the total deposition of odorants on various regions of the nasal mucosa. This requires estimating the proper value

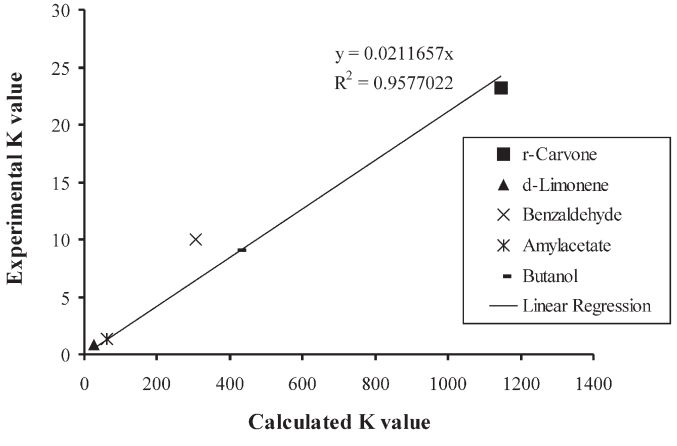

Figure 7 Plot of experimental fitted dimensionless K_{exp} values (low flow rate, 3.33 l/min at 20 s) against calculated K_{cal} values for five odorants with known mucosa solubility.

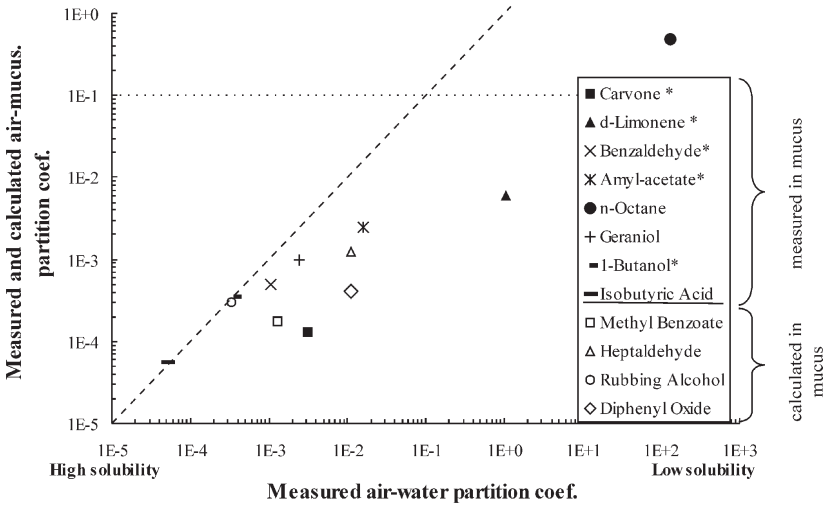

Figure 8 Plot of experimentally measured (Hornung *et al.*) and calculated (last four empty symbols, low flow rate, 3.33 l/min at 20 s) air/mucus partition coefficients against measured air/water partition coefficient. Odorants marked with * are those whose experimental air/mucus partition coefficient data were used to obtain a_K.

of the dimensionless mucosal transport parameter K. The first step is to estimate β_{real} from β_{water} using Figure 8 as an approximate 'universal curve', which should be reasonably accurate for molecules of similar structure. The next step is to substitute β_m^{real} into the last term in equation (4) to obtain an estimate of K^{exp} using a known value of a_k for the relevant flow rate. This estimated value of K^{exp} is a great improvement over K^{cal}, which involves only water values of the parameters.

Conclusion

Combining physical measurements with modern CFD techniques has allowed for a better description of the factors that govern steady state odorant nasal mucosal deposition. It is hoped that this description will lead to a better understanding of odorant uptake and diffusive transport processes in the human nasal mucosal layer. The results suggest that odorant transport in the human nasal mucosa differs from that observed in a thin layer of water in two important aspects. First, there seems to be a non-odorant-dependent increase in effective diffusive resistance of the olfactory mucosa as compared to that in water. Secondly, there are differences in air/mucus solubility as compared to the air/water solubility. Accurate quantification of these two processes is valuable for future numerical simulations of odorant transport in the human nasal cavity and will allow for a more full appreciation of odorant uptake by the olfactory mucosa.

Acknowledgements

The authors wish to thank Jason Newlon and Casey Schofield for their assistance in methods development and Scott Spicer for excellent technical assistance. The authors also wish to thank two anonymous reviewers for their timely and careful comments.

References

Getchell, **T.V., Margolis, T.V.** and **Getchell, M.L.** (1984) *Perireceptor and receptor events in vertebrate olfaction*. Prog. Neurobiol., 23, 317–345.

Hahn, **I., Scherer, P.W.** and **Mozell, M.M.** (1994) *A mass transport model of olfaction*. J. Theor. Biol., 167, 115–128.

Hornung, **D.E.** and **Mozell, M.M.** (1977) *Factors influencing the differential sorption of odorant molecules across the olfactory mucosa*. J. Gen. Physiol., 69, 343–361.

Hornung, **D.E.** and **Mozell, M.M.** (1981) *Accessibility of odorant molecules to the receptors.* In Cagan, R.H. and Kare, M.R. (eds), Biochemistry of Taste and Olfaction. Academic Press, New York, pp. 33–45.

Hornung, **D.E., Mozell, M.M.** and **Serio, J.A.** (1980) *Olfactory mucus/air partitioning of odorant.* In van der Starre, H. (ed.), Olfaction and Taste VII. IRL Press, London, pp. 167–170.

Hornung, **D.E., Youngentob, S.L.** and **Mozell, M.M.** (1987) *Olfactory mucosa/air partitioning of odorants*. Brain Res., 413, 147–154.

Howard, **P.H., Meylan, W.M.** and **Fake, F.F.** (1997) Handbook of Physical Properties of Organic Chemicals, 1st edn. CRC Press/Lewis Publishers, Boca Raton, FL.

Kent, **P.F., Mozell, M.M., Murphy, S.J.** and **Hornung, D.E.** (1996) *The interaction of imposed and inherent olfactory mucosal activity patterns and their composite representation in a mammalian species using voltage-sensitive dyes*. J. Neurosci., 16, 345–353.

Keyhani, **K., Scherer, P.W.** and **Mozell, M.M.** (1995) *Numerical simulation of airflow in the human nasal cavity*. J. Biomech. Eng., 117, 429–441.

Keyhani, **K., Scherer, P.W.** and **Mozell, M.M.** (1997) *A numerical model of nasal odorant transport for the analysis of human olfaction*. J. Theor. Biol., 186, 279–301.

Mozell, **M.M.** (1970) *Evidence for a chromatographic model of olfaction*. J. Gen. Physiol., 56, 46–63.

Mozell, **M.M.** and **Hornung, D.E.** (1985) *Peripheral Mechanisms in the Olfactory Process.* In Pfaff, D. (ed.), Taste, Olfaction, and the Central

Nervous System. The Rockefeller University Press, New York, pp. 253–297.

Mozell, **M.M.** and **Jagodowicz, M.** (1973) *Chromatographic separation of odorants by the nose: retention times measured across* in vivo *olfactory mucosa*. Science, 181, 1247–1249.

Mozell, **M.M., Sheehe, P.R., Hornung, D.E., Kent, P.F., Youngentob, S.L.** and **Murphy, S.J.** (1987) *Imposed and inherent mucosal activity patterns. Their composite representation of olfactory stimuli*. J. Gen. Physiol., 90, 625–650.

Orozco, **M.** and **Luque, F.J.** (2000) *Theoretical methods for the description of the solvent effect in biomolecular systems*. Chem. Rev., 100, 4187–4225.

Pelosi, **P.** (1994) *Odorant-binding proteins*. Crit. Rev. Biochem. Mol. Biol., 29, 199–228.

Subramaniam, **R.P., Richardson, R.B., Morgan, K.T.** and **Kimbell, J.S.** (1999) *Computational fluid dynamics simulations of inspiratory airflow in the human nose and nasopharynx*. Inhal. Toxicol., 10, 91–120.

Walker, **J.C., Kurtz, D.B., Shore, F.M., Ogden, M.W.** and **Walker, J.H., IV** (1990) *Apparatus for the automated measurement of the responses of humans to odorants.* Chem. Senses, 15, 165–177.

Welty, **J.R., Wicks, G.E.** and **Wilson, R.E.** (1976) Fundamentals of Momentum, Heat and Mass Transfer, 2nd edn. Wiley, New York.

Zhao, **K., Scherer, P.W., Hajiloo, S.A.** and **Dalton, P.** (2004) *Effect of anatomy on human nasal air flow and odorant transport patterns: implications for olfaction*. Chem. Senses, 29, 365–380.

Accepted August 30, 2004